Inorganic Chemistry

Article

pubs.acs.org/IC

Synthesis and Reactivity of the Unsaturated Trinuclear Phosphanido Complex $[(C_6F_5)_2Pt(\mu\text{-}PPh_2)_2Pt(\mu\text{-}PPh_2)_2Pt(PPh_3)]$

Juan Forniés,[‡] Consuelo Fortuño,*[,‡] Susana Ibáñez,[‡] Antonio Martín,[‡] Piero Mastrorilli,*[,§] Vito Gallo,[§] and Athanassios Tsipis*[,⊥]

[‡]Departamento de Química Inorgánica, Instituto de Síntesis Química y Catálisis Homogénea, Universidad de Zaragoza, CSIC, 50009 Zaragoza, Spain

[§]Dipartimento di Ingegneria Civile, Ambientale, del Territorio, Edile e di Chimica (DICATECh), Politecnico di Bari, via Orabona 4, I-70125 Bari, Italy

[⊥]Laboratory of Inorganic and General Chemistry, Department of Chemistry, University of Ioannina, 45110 Ioannina, Greece

Supporting Information

ABSTRACT: The reaction of $[NBu_4][(C_6F_5)_2Pt(\mu\text{-}PPh_2)_2Pt(\mu\text{-}PPh_2)_2Pt(O,O\text{-acac})]$ (48 VEC) with $[HPPh_3][ClO_4]$ gives the 46 VEC unsaturated $[(C_6F_5)_2Pt^1(\mu\text{-}PPh_2)_2Pt^2(\mu\text{-}PPh_2)_2Pt^3(PPh_3)]$ (Pt^2–Pt^3) (**1**), a trinuclear compound endowed with a Pt–Pt bond. This compound displays amphiphilic behavior and reacts easily with nucleophiles L, yielding the saturated complexes $[(C_6F_5)_2Pt^{II}(\mu\text{-}PPh_2)_2Pt^{II}(\mu\text{-}PPh_2)_2Pt^{II}(PPh_3)L]$ [L = PPh_3 (**2**), py (**3**)]. The reaction with the electrophile $[Ag(OClO_3)PPh_3]$ affords the adduct **1**·$AgPPh_3$, which evolves, even at low temperature, to a mixture in which $[(C_6F_5)_2Pt^{III}(\mu\text{-}PPh_2)_2Pt^{III}(\mu\text{-}PPh_2)_2Pt^{II}(PPh_3)_2]^{2+}$ (Pt^{III}–Pt^{III}) and **2** (plus silver metal) are present. The nucleophilic nature of **1** is also demonstrated through its reaction with *cis*-$[Pt(C_6F_5)_2(THF)_2]$, which results in the formation of $[Pt_4(\mu\text{-}PPh_2)_4(C_6F_5)_4(PPh_3)]$ (**4**). The structure and NMR features indicate that **1** can be better considered as a Pt^{II}–Pt^{III}–Pt^{I} complex instead of a Pt^{II}–Pt^{II}–Pt^{II} derivative. Theoretical calculations (density functional theory) on similar model compounds are in agreement with the assigned oxidation states of the metal centers. The strong intermetallic interactions resulting in a Pt^2–Pt^3 metal–metal bond and the respective bonding mechanism were verified by employing a multitude of computational techniques (natural bond order analysis, the Laplacian of the electron density, and localized orbital locator profiles).

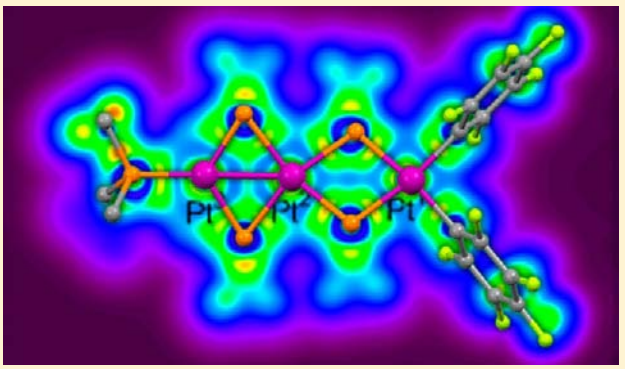

INTRODUCTION

The ability of the phosphanido ligands to stabilize polynuclear complexes because of their ability to form very stable M–P bonds is well-known. The PR_2 groups usually act as bridging ligands and display a great geometrical flexibility, which allows diorganophosphanides to bridge metal centers across a wide range of M–M distances.[2−9]

We are engaged in the synthesis of polynuclear platinum and/or palladium phosphanido complexes, and the judicious choice of the starting materials and reaction processes has allowed the rational synthesis of phosphanido complexes of different nuclearity with or without a metal–metal bond, with the latter depending on the total valence electron count (VEC).[10−29] Typically, polynuclear platinum or palladium complexes that contain 16 electrons per metal center, i.e., a VEC of 16*n* (*n* = number of metal centers), are considered to be saturated and do not require the presence of any metal–metal bond. For instance, in binuclear phosphanido complexes studied by us, the elimination of a pair of electrons, either via one-electron oxidation of each metal center or by elimination of one ligand, results in both cases in the formation of a Pt–Pt bond.[10,13,29,30] When a ligand is eliminated in the resulting binuclear complex, one of the Pt centers is only three-coordinated.

In this paper, we report a combined experimental and theoretical study on the unsaturated trinuclear complex $[(C_6F_5)_2Pt^1(\mu\text{-}PPh_2)_2Pt^2(\mu\text{-}PPh_2)_2Pt^3(PPh_3)]$ (Pt^2–Pt^3) (**1**), from which we concluded that **1** should be better considered a Pt^{II}–Pt^{III}–Pt^{I} complex instead of a Pt^{II}–Pt^{II}–Pt^{II} one. The reactivity of **1** toward representative nucleophiles and electrophiles is also reported.

RESULTS AND DISCUSSION

We have recently reported that the trinuclear saturated (48 VEC) acetylacetonato complex $[NBu_4][(C_6F_5)_2Pt(\mu\text{-}PPh_2)_2Pt(\mu\text{-}PPh_2)_2Pt(O,O\text{-acac})]$ (**A**) reacts with $HClO_4$(aq) in acetonitrile, forming the trinuclear saturated $[(C_6F_5)_2Pt(\mu$-

Received: October 4, 2012
Published: January 28, 2013

   dx.doi.org/10.1021/ic3021639 | Inorg. Chem. 2013, 52, 1942−1953

Scheme 1

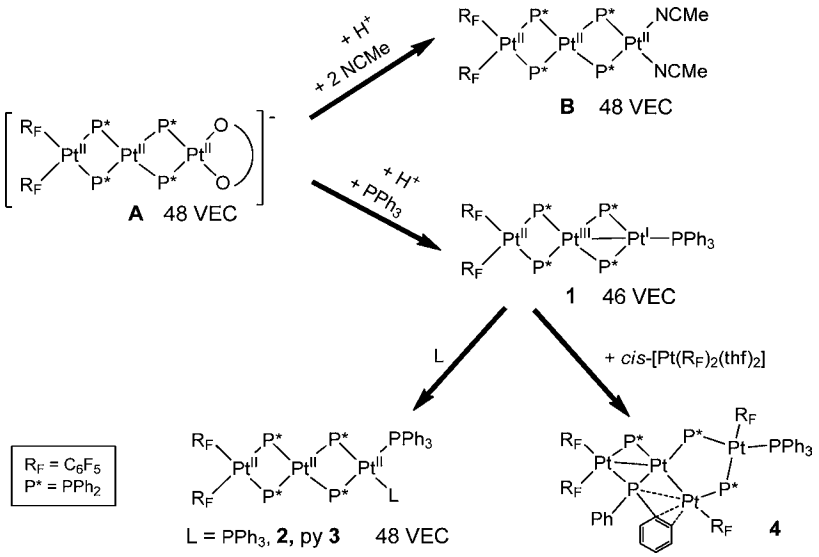

$PPh_2)_2Pt(\mu\text{-}PPh_2)_2Pt(NCCH_3)_2]$ (**B**) as a result of the protonation of acetylacetonate, elimination of Hacac, and coordination of two molecules of acetonitrile (Scheme 1).[31] When protonation of **A** was carried out with $[PPh_3H][ClO_4]$ in a noncoordinating solvent, the pale-yellow color of the solution turned instantaneously red, and from the reaction mixture, the unsaturated trinuclear complex (46 VEC) **1** could be crystallized. The unsaturated nature of this complex requires that a Pt−Pt bond be formed.[32]

The structure of **1** was determined by X-ray diffraction methods and is reported in Figure 1, with the most relevant

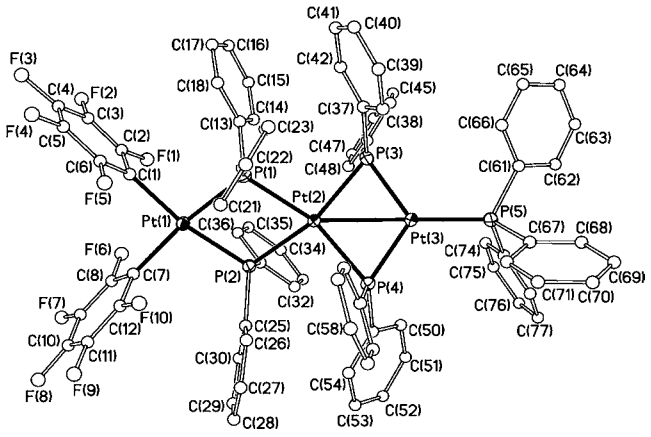

Figure 1. View of the molecular structure of **1**.

bond distances and angles listed in Table 1. Complex **1** is a trinuclear species, with the three Pt atoms forming an almost linear array [the value of the Pt(1)−Pt(2)−Pt(3) angle is 178.14(1)°]. The coordination environment of Pt(1) is square-planar, with two pentafluorophenyl ligands mutually cis and two phosphanido ligands bridging Pt(1) and Pt(2). The Pt(1)···Pt(2) distance is 3.6760(4) Å, excluding any intermetallic interaction. Accordingly, the Pt(1)−P(1)−Pt(2) and Pt(1)−P(2)−Pt(2) angles are broad (ca. 105°; Table 1). The Pt(2) environment is more distorted, with a coordination sphere that can be described as intermediate between square-planar and tetrahedral. The dihedral angle between the P(1)−Pt(2)−P(2) and P(3)−Pt(2)−P(4) planes is 31.60(6)°, and the P−Pt(2)−P angles deviate significantly from the ideal values of 90 or 180° (see Table 1). As expected, on the basis of the number of skeletal electrons (46 VEC), Pt(2) is bonded to Pt(3) with a bond distance of 2.6985(4) Å, a value in the range expected for a Pt−Pt bond.[28,32,33] The smaller values of the Pt(2)−P(3)−Pt(3) and Pt(2)−P(4)−Pt(3) angles compared to the analogues involving P(1) and P(2) (see Table 1) are in agreement with the presence of the intermetallic Pt−Pt bond. It is worth noting that the environment of Pt(3) is formally three-coordinated and lies in the center of an almost equilateral triangle formed by the three P atoms bonded to it. The P(5) atom of the triphenylphosphane ligand is located practically in the same line formed by the three Pt atoms, with a Pt(2)−Pt(3)−P(5) angle of 173.05(5)°. The geometry around Pt(3) is identical with that found for phosphanidoplatinum(I) complexes bonded to terminal phosphanes (or phosphinites) and bridged by diorganophosphanides of the general formula $[(PR^1{}_2R^2)Pt(\mu\text{-}PR^3{}_2)_2Pt(PR^4{}_2R^5)](Pt{-}Pt)$ ($R^1 = R^2 = R^4 = R^5$ = Me, R^3 = ^{t}Bu; $R^1 = R^2 = R^4 = R^5$ = Ph, R^3 = ^{t}Bu;[34] $R^1 = R^4$ = Me, $R^2 = R^5$ = OMe, R^3 = *cyclo*-C_6H_{11};[5] $R^1 = R^2 = R^3 = R^4 = R^5$ = Ph).[35] Considering that the geometry of Pt(2) is reminiscent of that of the known phosphanido-bridged Pt^{III} atoms, i.e., $Pt^{1/2}$ in $[(C_6F_5)_2Pt^1(\mu\text{-}PPh_2)_2Pt^2(C_6F_5)_2](Pt{-}Pt)$,[10] $[(C_6F_5)_2Pt^1(\mu\text{-}PPh_2)_2Pt^2(\mu\text{-}PPh_2)_2Pt^3(O,O\text{-}acac)](Pt^1{-}Pt^2)^+$,[31] and $[(C_6F_5)_2Pt^1(\mu\text{-}PPh_2)_2Pt^2(\mu\text{-}PPh_2)_2Pt^3(C_6F_5)_2](Pt^1{-}Pt^2)$,[36] the following hypothesis can be put forward: complex **1** should be better regarded as a $Pt^{II}{-}Pt^{III}{-}Pt^{I}$ species rather than a $Pt^{II}{-}Pt^{II}{-}Pt^{II}$ complex. Given that such a hypothesis might be substantiated by analysis of the ^{195}Pt NMR features, we decided to compare the ^{195}Pt data for **1** with those of the known Pt^{I} and Pt^{III} systems.

Because of the low sensitivity of the ^{195}Pt nucleus and the very large range of values for $\delta_{^{195}Pt}$,[37] detection of all ^{195}Pt signals of a polynuclear compound requires the particularly time-consuming process of registering several spectra, to span all spectral windows where the ^{195}Pt signals are thought to fall. In addition, the broadness of some signals lowers their S/N ratio, thus hampering their detection. To overcome this drawback, the ^{195}Pt resonances of **1** were recorded by means of $^{19}F{-}^{195}Pt$ and $^{1}H{-}^{195}Pt$ heteronuclear multiple-quantum

dx.doi.org/10.1021/ic3021639 | Inorg. Chem. 2013, 52, 1942−1953

Table 1. Selected Bond Lengths (Å) and Angles (deg) for $[(C_6F_5)_2Pt(\mu\text{-}PPh_2)_2Pt(\mu\text{-}PPh_2)_2Pt(PPh_3)]\cdot 0.25CHCl_3\cdot 0.25C_6H_{14}$ ($1\cdot 0.25CHCl_3\cdot 0.25C_6H_{14}$)

Pt(1)−C(7)	2.052(6)	Pt(1)−C(1)	2.064(7)	Pt(1)−P(1)	2.2706(18)
Pt(1)−P(2)	2.2747(18)	Pt(2)−P(2)	2.3605(18)	Pt(2)−P(1)	2.3624(18)
Pt(2)−P(3)	2.3677(17)	Pt(2)−P(4)	2.3918(19)	Pt(2)−Pt(3)	2.6985(4)
Pt(3)−P(3)	2.2181(19)	Pt(3)−P(5)	2.2254(18)	Pt(3)−P(4)	2.2306(17)
C(7)−Pt(1)−C(1)	91.3(2)	P(3)−Pt(3)−P(5)	122.50(6)	P(2)−Pt(2)−P(4)	95.94(6)
C(1)−Pt(1)−P(1)	95.38(18)	P(5)−Pt(3)−P(4)	123.55(7)	P(3)−Pt(2)−P(4)	102.95(6)
C(1)−Pt(1)−P(2)	167.87(18)	Pt(1)−P(2)−Pt(2)	104.93(7)	P(1)−Pt(2)−Pt(3)	143.50(4)
P(2)−Pt(2)−P(1)	73.27(6)	Pt(3)−P(4)−Pt(2)	71.34(5)	P(4)−Pt(2)−Pt(3)	51.55(4)
P(1)−Pt(2)−P(3)	95.76(6)	C(7)−Pt(1)−P(1)	169.17(19)	P(3)−Pt(3)−P(4)	113.64(7)
P(1)−Pt(2)−P(4)	153.10(6)	C(7)−Pt(1)−P(2)	97.97(18)	Pt(1)−P(1)−Pt(2)	105.00(7)
P(2)−Pt(2)−Pt(3)	143.23(4)	P(1)−Pt(1)−P(2)	76.64(6)	Pt(3)−P(3)−Pt(2)	72.01(5)
P(3)−Pt(2)−Pt(3)	51.42(5)	P(2)−Pt(2)−P(3)	154.56(7)		

coherence (HMQC) NMR experiments, which are faster than 1D $^{195}Pt\{^1H\}$ NMR experiments because of the higher sensitivity and abundance of the ^{19}F and ^1H nuclei.

Thus, the ^{195}Pt resonance of Pt^1 for **1** (δ −3712) was revealed by recording a $^{19}F-^{195}Pt$ HMQC NMR spectrum (Figure 2), exploiting the strong scalar coupling ($^3J_{F,Pt}$ = 312 Hz) between the *o*-F of the pentafluorophenyl rings and Pt^1. On the other hand, the Pt^2 and Pt^3 signals of **1** (δ −4720 and −5228, respectively) were obtained by recording a $^1H-^{195}Pt$ HMQC NMR spectrum (Figure 3), which was set to exploit the scalar coupling between the *o*-H of the phenyl rings and Pt atoms. Once the chemical shifts of each of the three ^{195}Pt signals were located, their fine structures were obtained by recording a 1D $^{195}Pt\{^1H\}$ NMR spectrum (Figure S1 in the Supporting Information), which showed inter alia a coupling constant between Pt^2 and Pt^3 of 515 Hz.

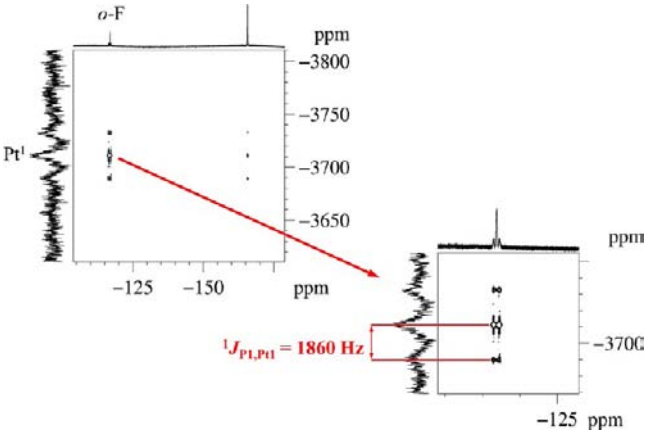

Figure 2. Portions of the $^{19}F-^{195}Pt$ HMQC NMR spectrum of **1** ($CDCl_3$, 298 K).

The chemical shift values observed for **1** substantiate our hypothesis on the $Pt^{II}-Pt^{III}-Pt^{I}$ oxidation states of the Pt atoms in **1**. In fact, while the chemical shift of Pt^1 is not greatly affected on passing from $[(C_6F_5)_2Pt^1(\mu\text{-}PPh_2)_2Pt^2(\mu\text{-}PPh_2)_2Pt^3(O,O\text{-acac})]^-$ (δ_{Pt^1} −3793) to the unsaturated **1** (δ_{Pt^1} −3712), the Pt^2 atom experienced a high shielding (from δ_{Pt^2} −3894 to δ_{Pt^2} −4720), which has already been observed upon Pt^{II} to Pt^{III} oxidation of phosphanido-bridged polynuclear complexes,[31] and the chemical shift of Pt^3 for **1** (δ_{Pt^3} −5228) is perfectly in the −5000 to −6000 ppm range of the known phosphanido-bridged Pt^I complexes[2] (the chemical shift of Pt^3 in the precursor is δ_{Pt^3} −3159).

The same argument (i.e., the occurrence of a Pt^I-Pt^{III} system instead of a $Pt^{II}-Pt^{II}$ one) might be thought to apply to complex $[(C_6F_5)_2Pt^1(\mu\text{-}PPh_2)_2Pt^2PPh_3](Pt^1-Pt^2)$ (**C**), for which the geometric parameters of Pt^1 and Pt^2 perfectly fit those of Pt^{III} and Pt^I phosphanido-bridged atoms, respectively. The ^{195}Pt NMR signals of **C** were found at δ_{Pt^1} −5369 and δ_{Pt^2} −5354, with a $^1J_{Pt,Pt}$ of 407 Hz, while the corresponding data for its precursor $[(C_6F_5)_2Pt^1(\mu\text{-}PPh_2)_2Pt^2(O,O\text{-acac})]$ are δ_{Pt^1} −3236 and δ_{Pt^2} −3934. This confirms our previous observation[31] that ^{195}Pt chemical shifts of phosphanido-bridged polynuclear complexes are strongly dependent on the geometry

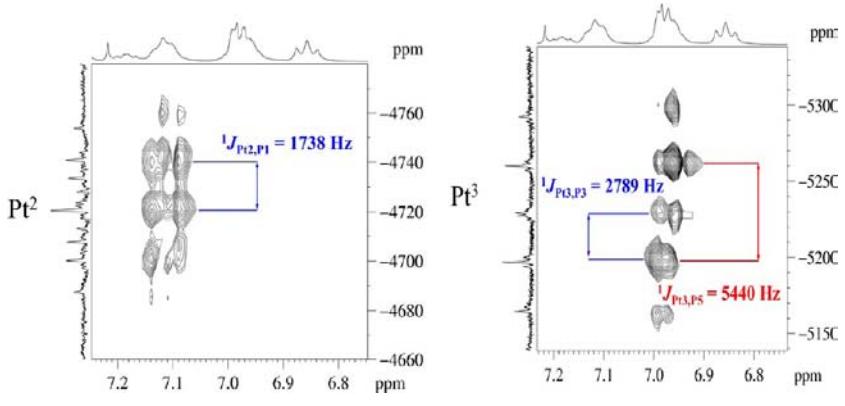

Figure 3. Portions of the $^1H-^{195}Pt$ HMQC NMR spectrum of **1** ($CDCl_3$, 298 K).

dx.doi.org/10.1021/ic3021639 | Inorg. Chem. 2013, 52, 1942−1953

around the Pt atom, with the presence of the Pt_2P_2 ring endowed with a Pt−Pt bond resulting in ^{195}Pt NMR signals high-field-shifted with respect to their analogues for a Pt_2P_2 ring *not* endowed with a Pt−Pt bond. As can be seen below, the ^{195}Pt chemical shifts of **1** show the same tendency as the ^{195}Pt chemical shifts calculated for the model complexes.

The $^{31}P\{^1H\}$ NMR spectrum of **1** in deuterochloroform showed three signals according to the presence of three different types of P atoms. The spectrum shows a low-field signal centered at δ 236.7 due to the P atoms of the PPh_2 groups (P^3 and P^4) bridging two Pt atoms (Pt^2 and Pt^3) subtending a metal−metal bond, a signal centered at δ 42.5 assigned to the PPh_3 ligand (P^5), and a high-field signal at δ −158.9 due to the P atoms of the other two PPh_2 groups (P^1 and P^2). The $^{31}P\{^1H\}$ correlation spectroscopy (COSY) NMR

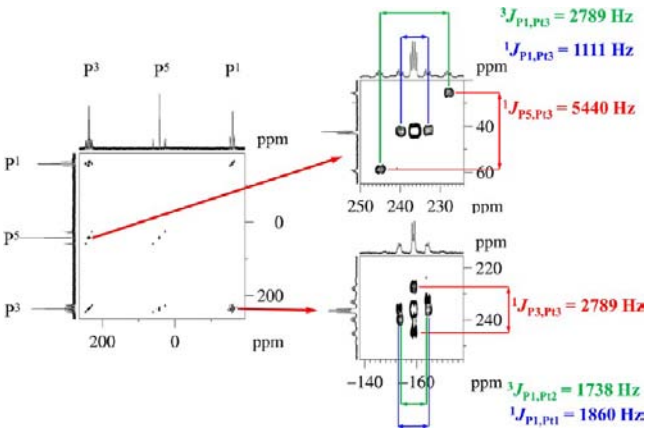

Figure 4. Portions of the $^{31}P\{^1H\}$ COSY NMR spectrum of **1** ($CDCl_3$, 298 K).

spectrum (Figure 4) allowed us to unequivocally determine the $^{31}P-^{195}Pt$ coupling constants that were not directly extractable from 1D $^{31}P\{^1H\}$ NMR spectra because of overlapping of the ^{195}Pt satellites. All signals appear as complex multiplets because of the second-order spin systems to which this molecule belongs at a field of 161 MHz. The ^{31}P features of **1** (Table 2) were determined by computer simulation of the AA′XX′M (29.0%), AA′XX′MZ (14.8% for each of the three isotopomers), and AA′XX′MZY (7.6% for each of the three isotopomers) spin systems (A, X, and M = ^{31}P; Y and Z = ^{195}Pt) using as starting chemical shifts and coupling constants those extractable directly from the experimental $^{31}P\{^1H\}$ and $^{31}P\{^1H\}$ COSY NMR spectra.

Table 2. NMR Parameters for 1 ($CDCl_3$, 298 K)[a]

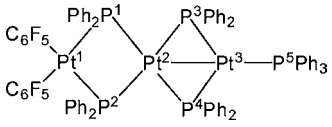

	P^1 [b]	P^3 [c]	P^5	Pt^1	Pt^2	Pt^3
P^1	**−158.9**	45	8	1860	1738	15
P^3		**236.7**	72		1111	2789
P^5			**42.5**		32	5440
Pt^1				**−3712**		
Pt^2					**−4720**	515
Pt^3						**−5228**

[a]Chemical shifts (bold typeface) are in parts per million; coupling constants (normal type) are in hertz. [b]$^2J_{P(1),P(2)}$ = 150 Hz. [c]$^2J_{P(3),P(4)}$ = 55 Hz; $^2J_{P(1),P(4)}$ = 125 Hz.

The comparison between the calculated and experimental $^{31}P\{^1H\}$ NMR spectra is shown in Figure S2 in the Supporting Information. The value of 45 Hz calculated for the coupling constant between P^1 and P^3 (or P^2 and P^4), which is higher than those expected for *cis*-P ligands in a square-planar geometry (J_{cis} < 20 Hz),[38] indicates that the geometry of Pt^2 found in the solid state (which we have described as intermediate between square-planar and tetrahedral) is maintained in solution.

Reactivity of 1 toward Nucleophiles or Electrophiles. Unsaturated complexes analogous to **1** were shown to be able to react with nucleophiles, producing saturated derivatives (16*n* VEC, where *n* is the number of Pt, or Pd, atoms present in the molecule; Scheme 2).[30] Thus, the reaction of **1** with PPh_3 or

Scheme 2

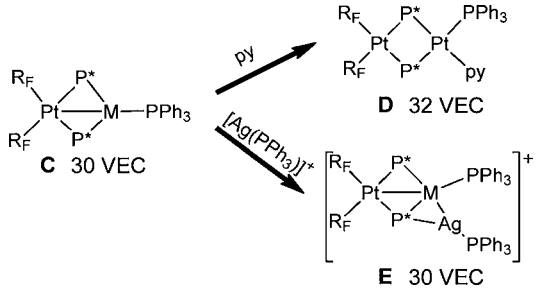

pyridine in CH_2Cl_2 resulted in a sudden red-to-yellow color change of the solution from which a yellow solid formulated as $[(C_6F_5)_2Pt(\mu\text{-}PPh_2)_2Pt(\mu\text{-}PPh_2)_2Pt(PPh_3)L]$ [L = PPh_3 (**2**),[28] py (**3**); Scheme 1] was isolated. Unfortunately, **2** and **3** are very insoluble in all common organic solvents, precluding a complete characterization. In all likelihood, the saturated complexes **2** and **3** do not display M−M bonds as for $[NBu_4][(C_6F_5)_2Pt(\mu\text{-}PPh_2)_2Pt(\mu\text{-}PPh_2)_2Pt(acac)]$.[31]

On the other hand, we have shown that in complex $[(C_6F_5)_2Pt^1(\mu\text{-}PPh_2)_2Pt^2(PPh_3)]$ (**C**) the μ-P−Pt^2 bond is electron-rich and reacts with electrophiles such as $AgPPh_3^+$, giving trinuclear complexes with the Pt−Ag bond.[39] This behavior is in full agreement with the hypothesis of the different oxidation states of Pt^1(III) and Pt^2(I), thus more electron-rich. We have carried out the reaction of **1** with $[Ag(OClO_3)PPh_3]$ (1:1 molar ratio, room temperature) in dichloromethane, which resulted in the formation of a mixture of compounds and of a silver mirror. Multinuclear NMR spectroscopy revealed signals due to the previously reported[28] complex $[(C_6F_5)_2Pt^{III}(\mu\text{-}PPh_2)_2Pt^{III}(\mu\text{-}PPh_2)_2Pt^{II}(PPh_3)_2]^{2+}$ along with signals belonging to unidentified species. These findings indicate that the treatment of **1** with $AgPPh_3^+$ does not result in the formation of the 1:1 adduct **1**·$AgPPh_3$ displaying a Pt−P−Ag (three-center two-electron, 3c-2e) bond such as occurs in the case of the analogous dinuclear complex **C** (Scheme 2)[28,39] but in a redox process. When **1** was mixed with $[Ag(OClO_3)PPh_3]$ (1:1 molar ratio, dichloromethane) at 273 K and the resulting solution was immediately evaporated to dryness, a red solid was obtained, which was analyzed by ^{31}P and ^{19}F NMR spectroscopy. In the $^{31}P\{^1H\}$ NMR spectrum of the solid redissolved in CD_2Cl_2 at 193 K, beside the signals of $[(C_6F_5)_2Pt^{III}(\mu\text{-}PPh_2)_2Pt^{III}(\mu\text{-}PPh_2)_2Pt^{II}(PPh_3)_2]^{2+}$ and other unidentified

dx.doi.org/10.1021/ic3021639 | *Inorg. Chem.* 2013, 52, 1942−1953

Scheme 3

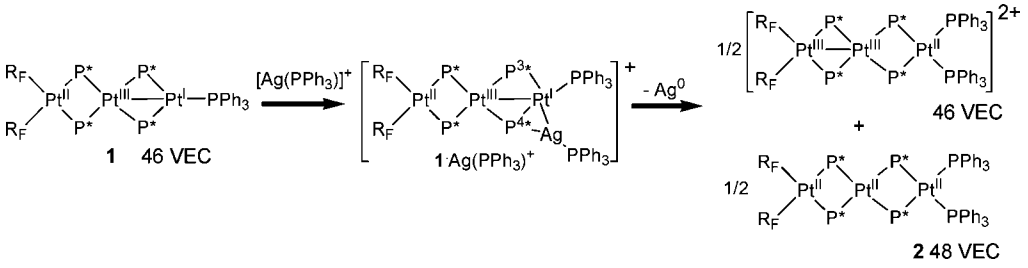

Scheme 4

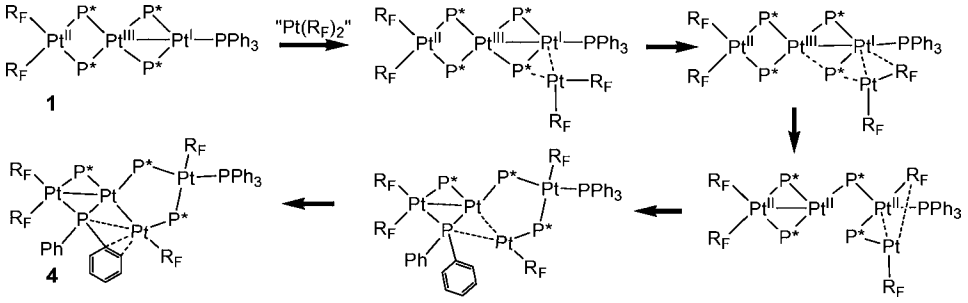

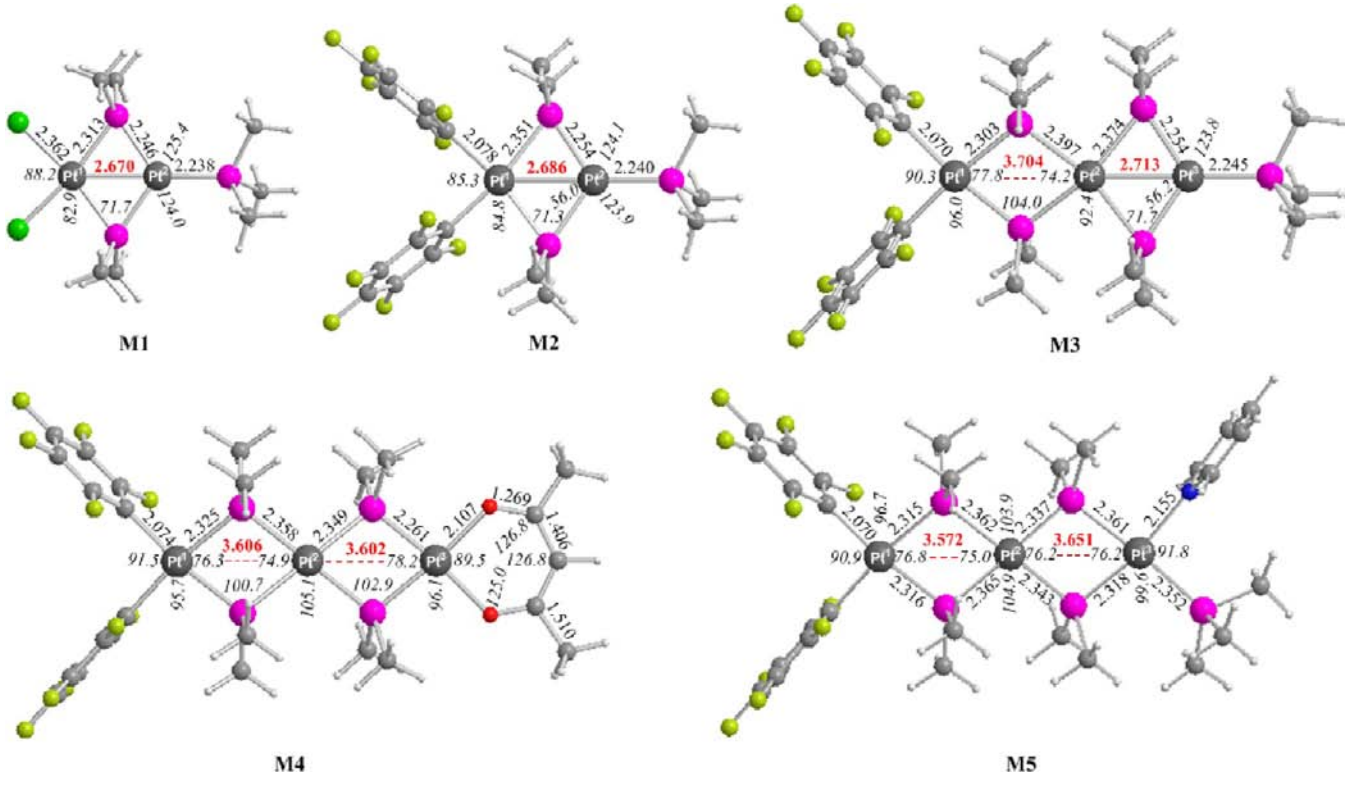

Figure 5. Equilibrium structures of the model compounds **M1**–**M5** computed at the PBE0/Def2-TZVP(Pt)U6-31+G(d,p)(X) level of theory.

species, two signals at δ 281 and δ 191 were assigned to P^3 and P^4, respectively, of the fragment of the type "Pt(μ-PPh_2)$_2$Pt-{Ag(PPh_3)}" (Scheme 3), in which a μ-P^4–Pt bond donates electron density to the Ag center (possibly the adduct [**1**·Ag(PPh_3)]$^+$. This indicates that, even though a 1:1 adduct **1**·$AgPPh_3$ could be initially formed, it evolves through a redox process to form the trinuclear [Pt^{III}–Pt^{III}–Pt^{II}]$^{2+}$ cation along with the saturated and insoluble complex **2**.

The electron-rich character of the Pt–P bond in **1** is clearly demonstrated by the reaction of **1** with *cis*-[Pt(C_6F_5)$_2$(THF)$_2$], a well-known Pt(C_6F_5)$_2$ synthon.[40,41] This reaction (1:1 molar ratio) in CH_2Cl_2 yielded [Pt_4(μ-PPh_2)$_4$(C_6F_5)$_4$(PPh_3)] (**4**), which had already been synthesized in our laboratories through a different process.[42] A plausible mechanism for the formation of **4** is shown in Scheme 4, in which the donor behavior of a μ-P–Pt bond is considered.[16,43,44]

dx.doi.org/10.1021/ic3021639 | *Inorg. Chem.* 2013, 52, 1942–1953

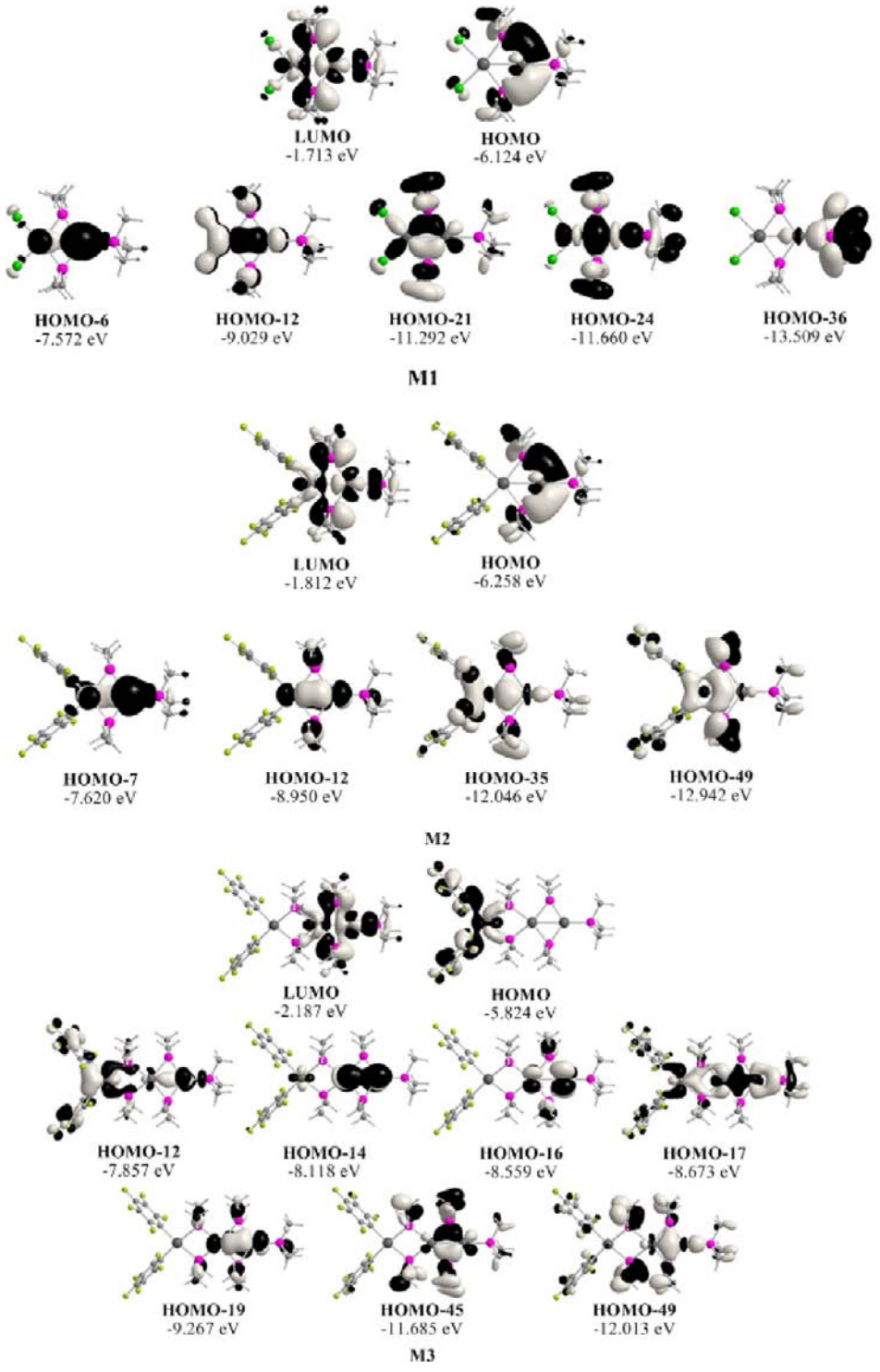

Figure 6. 3D contour plots of the HOMOs, LUMOs, and most relevant to the Pt−Pt bonding mode MOs in compounds **M1**−**M3**.

Electronic Properties and the Nature of the Intermetallic Pt−Pt Bond. In order to obtain a computationally convenient size for the compounds, we used models resulting upon substitution of the phenyl groups of the phosphanido ligands by methyl groups. To unveil the nature of the intermetallic Pt−Pt bond, we performed density functional theory (DFT) calculations on the dinuclear complexes $[(Cl_2Pt(\mu\text{-}PMe_2)_2Pt(PMe_3)]$ (**M1**) and $[(C_6F_5)_2Pt(\mu\text{-}PMe_2)_2Pt(PMe_3)]$ (**M2**), which exhibit strong intermetallic Pt···Pt interactions, and on the trinuclear model compounds $[(C_6F_5)_2Pt(\mu\text{-}PMe_2)_2Pt(\mu\text{-}PMe_2)_2Pt(PMe_3)]$ (**M3**), $[(C_6F_5)_2Pt(\mu\text{-}PMe_2)_2Pt(\mu\text{-}PMe_2)_2Pt(O,O\text{-acac})]^-$ (**M4**), and $[(C_6F_5)_2Pt(\mu\text{-}PMe_2)_2Pt(\mu\text{-}PMe_2)_2Pt(PMe_3)(py)]$ (**M5**) at the PBE0/Def2-TZVP(Pt)U6-31+G(d,p)(X) level. The optimized geometries of **M1**−**M5** are shown in Figure 5.

The equilibrium structures of the model systems **M3** and **M4** resemble those of the "real" complexes **1** and **A**, respectively, with the expected small structural variations due to the electronic and steric effects of the respective ligands. In general, the computed bond lengths of **M3** and **M4** model systems

dx.doi.org/10.1021/ic3021639 | *Inorg. Chem.* 2013, 52, 1942−1953

Scheme 5. Laplacian of the Electron Density, $\nabla^2\rho(\mathbf{r})$, Map on the *xy* Plane (Contour Value = 0.1) of the Model Compounds M1−M5[a]

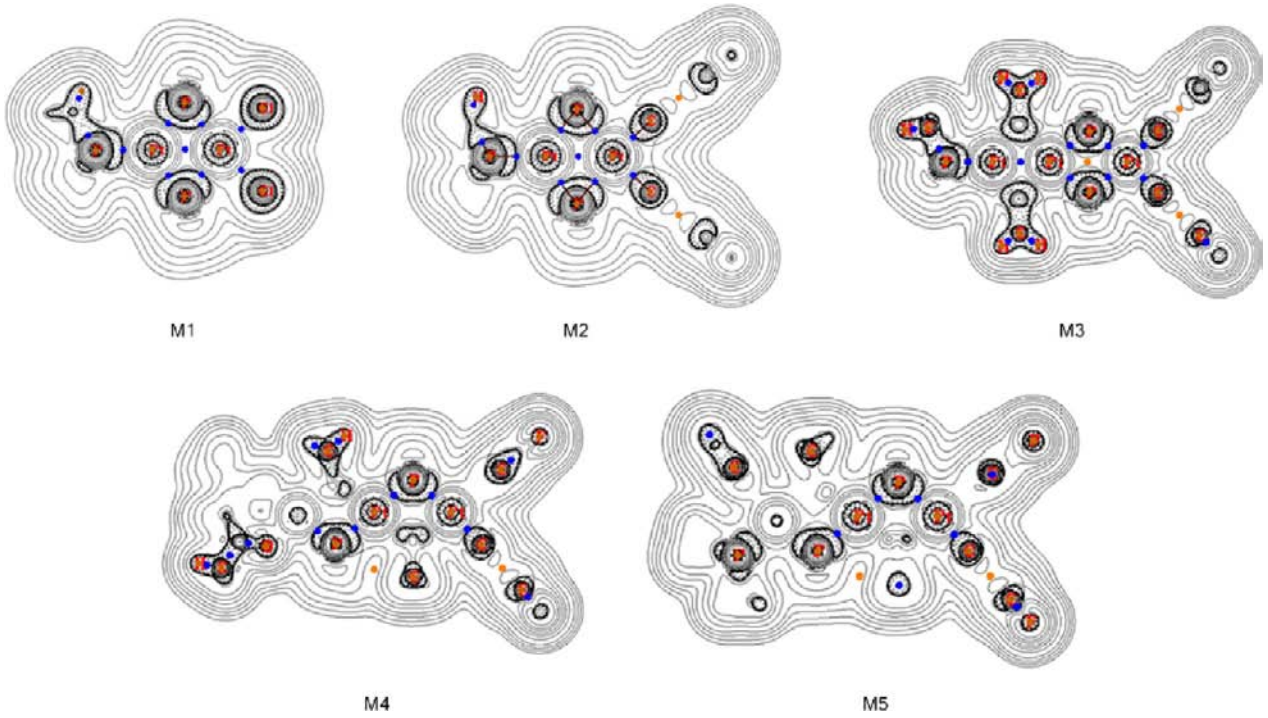

[a]Brown, blue, and orange circles denote (3, −3), (3, −1), and (3, +1) critical points, respectively.

exhibit elongation, in the ranges 0−0.036 and 0−0.045 Å, respectively, upon comparison to those obtained from X-ray structural analysis of **1** and **A**. On the other hand, deviations of the computed bond angles of **M3** and **M4** upon comparison with the respective X-ray analysis structural parameters fall within the ranges 0−3.5° and 0.3−2.4°, respectively. In the optimized geometries of all model compounds, the coordination environments of the central as well as terminal Pt atoms are planar. However, only in **M3**, the Pt metal centers are in an almost perfect linear alignment ($\angle Pt_1-Pt_2-Pt_3$ = 179.7°), while in the other two model compounds **M4** and **M5**, the $\angle Pt_1-Pt_2-Pt_3$ bond angles of the $Pt_1-Pt_2-Pt_3$ nuclear framework are estimated to be 174.1° and 170.3°.

Accordingly, in **M4** and **M5**, the coordination environments of the Pt metal centers adopt a "chair"-like conformation, while in **M3**, an almost coplanar orientation could be observed. It is worth noting that in the model compounds **M4** and **M5** the two Pt_2P_2 rhombuses are not planar, in contrast to those found for **M3**. In the latter, the planes of the two rhombuses form an angle equal to 49.8° with Pt−μ-P−Pt bridges in syn positions. The computed Pt−Pt distances are found to be well above the sum of the van der Waals radii of two Pt atoms (3.5 Å) with the exception of the Pt^2-Pt^3 distance in **M3**, which is estimated to be equal to 2.713 Å, in line with the X-ray structure analysis. This is indicative of a strong intermetallic interaction resulting in a Pt^2-Pt^3 metal−metal bond in **1** and in its model compound **M3**. Strong intermetallic interactions also exist in the compounds **M1** and **M2** exhibiting short Pt−Pt distances of 2.670 and 2.686 Å, respectively.

The highest occupied molecular orbital (HOMO) and the lowest unoccupied molecular orbital (LUMO) along with molecular orbitals (MOs) that are most relevant to the Pt−Pt bonding mode are shown in Figure 6. The HOMOs in the compounds **M1** and **M2** are localized on the coordination environment of Pt^2 and are constructed from bonding combinations of Pt $d_{x^2-y^2}$ atomic orbitals (AOs) with ligand group orbitals of the phosphanido bridging and phosphane ligands. On the other hand, the HOMO in **M3** is localized on the coordination environment of Pt^1 constructed from bonding combinations of Pt $d_{x^2-y^2}$ AOs with ligand group orbitals of the phosphanido bridging and C_6F_5 ligands. The LUMOs are located on the $Pt^1(\mu_2\text{-}PMe_2)Pt^2$ framework in **M1** and **M2** and on $Pt^2(\mu_2\text{-}PMe_2)Pt^3$ framework in **M3** involving overlap of PMe_3 p-type orbitals with 5d AOs of Pt centers. The Pt^1-Pt^2 bonding mechanism in **M1**−**M3** is reflected in the occupied MOs (Figure 6), which are of both σ- and π-type bonding MOs.

The Pt^1-Pt^2 bonding mode was further corroborated from the Laplacian of the electron density, $\nabla^2\rho(\mathbf{r})$, obtained from topological analysis performed by the atoms-in-molecules calculations (Scheme 5) introduced by Bader.[45]

Topological analysis involves the search for critical points, which are extremes in the 3D function $\rho(\mathbf{r})$, that is, points where $\nabla\rho(\mathbf{r})$ = (0, 0, 0). A set of trajectories of $\rho(\mathbf{r})$ terminating in the bond critical point (bcp) defines an interatomic surface that separates the basins of neighboring atoms. Trajectories connecting two atoms via the bcp describe the line of maximum density, which corresponds to bond paths in equilibrium geometry. The Laplacian of the electron density, $\nabla^2\rho(\mathbf{r})$, indicates relative charge concentrations [$\nabla^2\rho(\mathbf{r}) < 0$] and charge depletion [$\nabla^2\rho(\mathbf{r}) > 0$] in a molecule.

It is clear from Scheme 5 that there is charge concentration only between two out of the three Pt metal atoms. A bcp with (3, −1) signature was found in the midpoint between the two interacting Pt metal centers of the model compounds **M1**−**M3** (blue circles in Scheme 5). The Laplacian of the electron

dx.doi.org/10.1021/ic3021639 | *Inorg. Chem.* 2013, 52, 1942−1953

Scheme 6. Cut-Plane LOL Profiles of the Model Compounds M1−M5

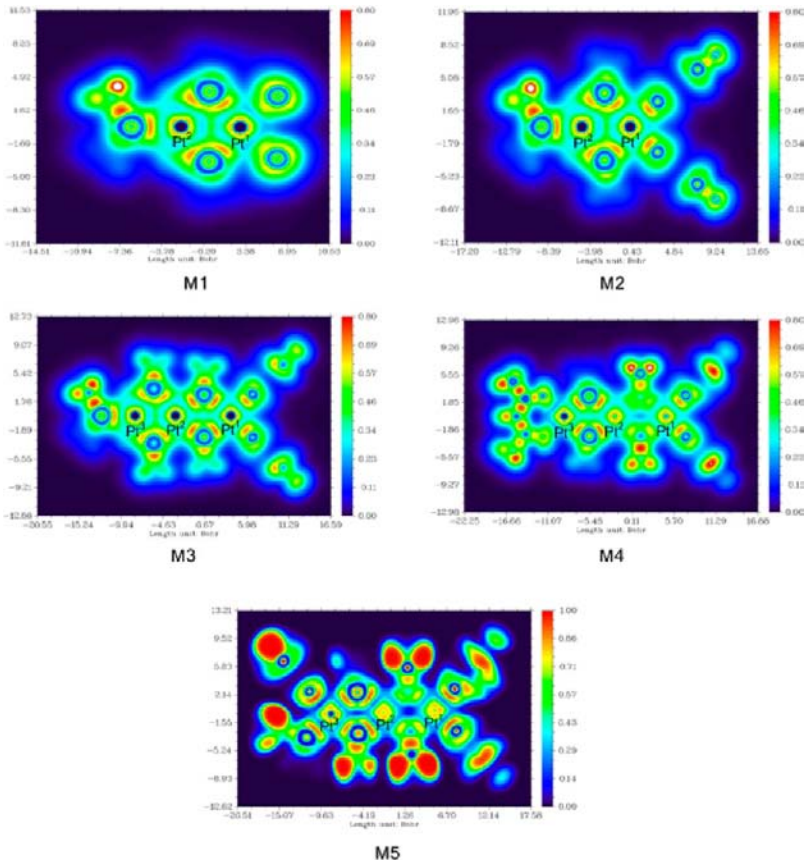

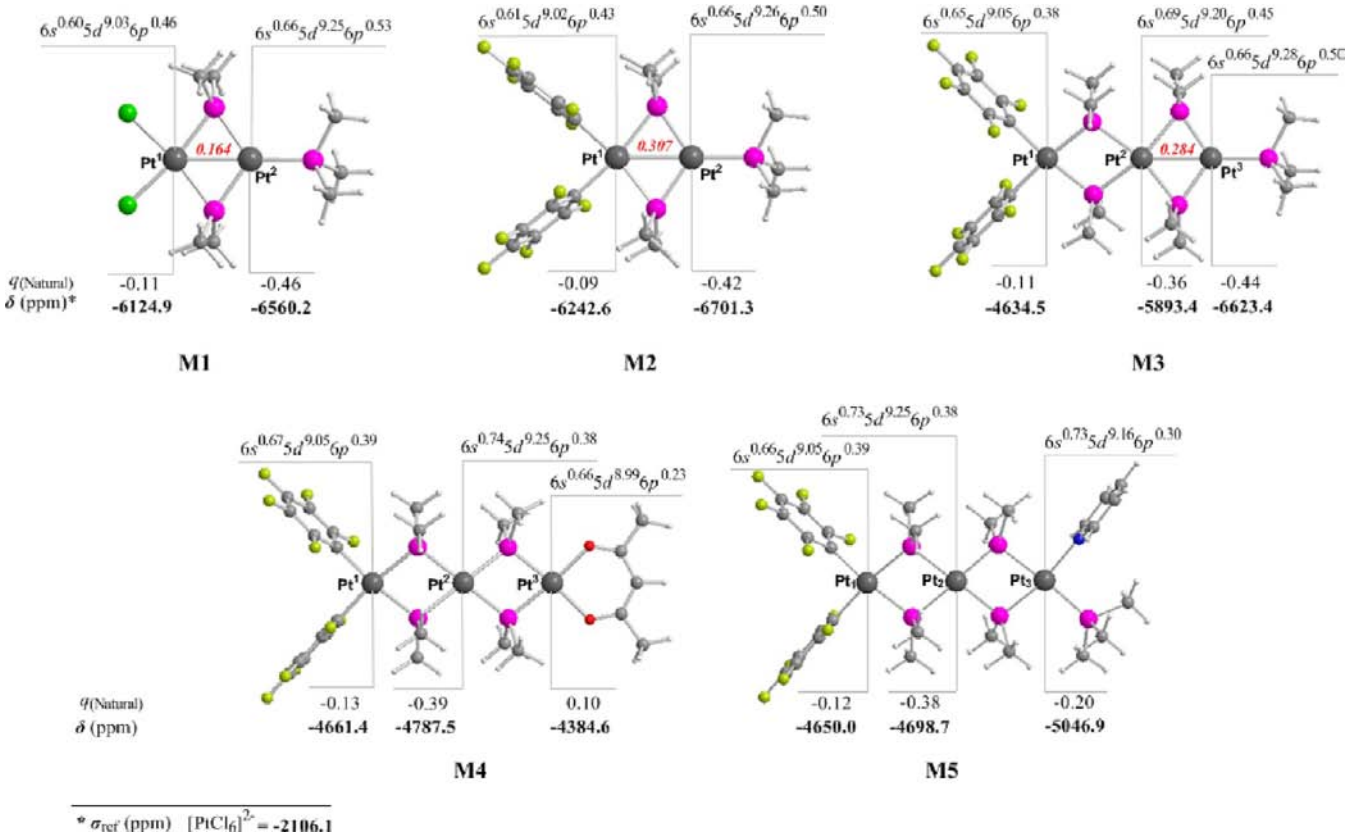

Figure 7. Data from NBO analysis along with the calculated ^{195}Pt chemical shifts for compounds **M1−M5**.

dx.doi.org/10.1021/ic3021639 | *Inorg. Chem.* 2013, 52, 1942−1953

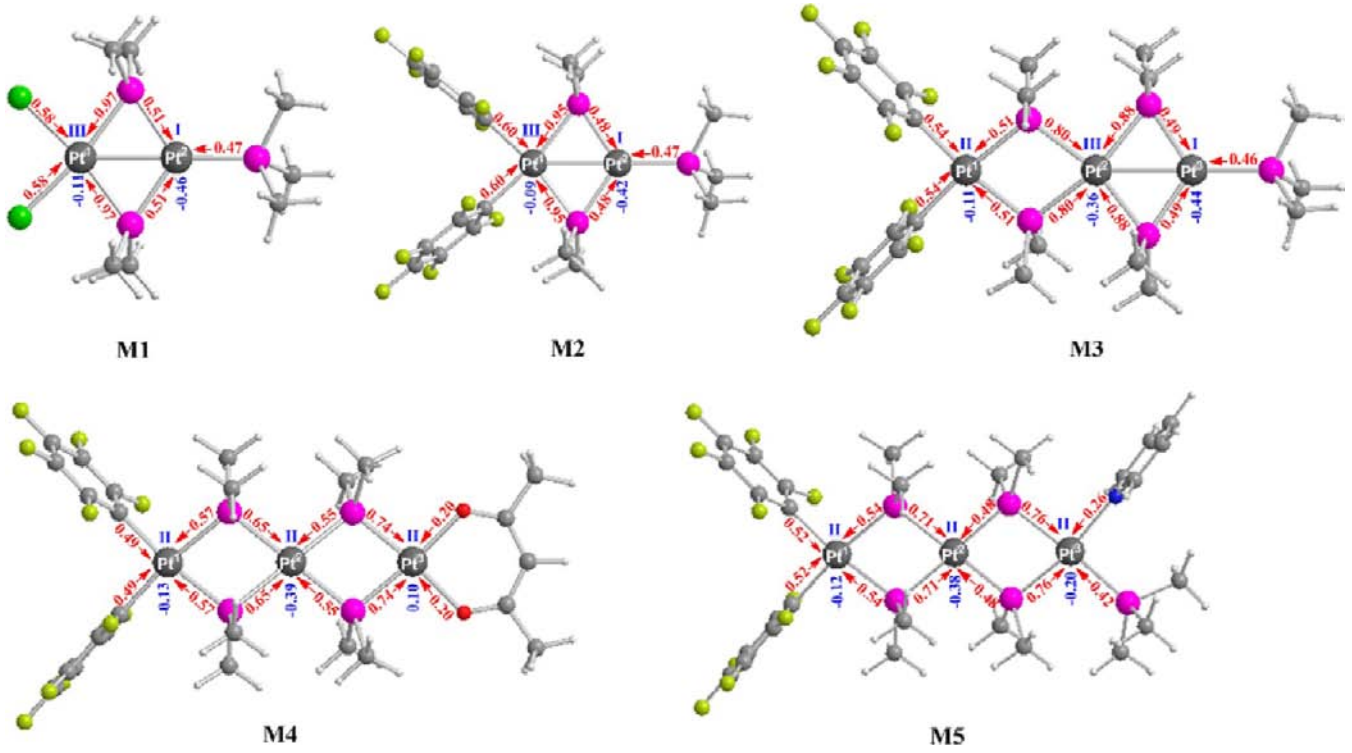

Figure 8. Natural charge transferred from the ligands to the metal centers in **M1**−**M5**.

density, $\nabla^2\rho(\mathbf{r})_{bcp}$, calculated for this bcp is small and negative (e.g., −0.0046 e Å^{-5} for **M3**), indicating a covalent interaction (also referred to as an "open-shell" or sharing interaction).[46] In contrast, between the central Pt metal atom paired with the Pt metal atom on the opposite site, only a ring critical point with (3, +1) signature could be observed (orange circle in Scheme 5).

The spatial organization of the bonding mechanism in the model compounds **M1**−**M5** can easily be recognized by the cut-plane localized orbital locator (LOL) profiles depicted in Scheme 6.

Identification of LOL basins such as atomic shells, bonds, and lone electron pairs is reflective[47,48] of the nature of the electronic structure of the investigated systems. The LOL function relies on consideration of the electron kinetic energy density and reveals slow electron regions compared to the uniform electron gas (LOL > 0.5). The slowest electron regions are located between the bonded atoms that correspond to a typical 2c-2e bonding situation (shown in yellow-red). The green LOL basins located between the interacting Pt−Pt atoms (LOL ≥ 0.5) are typical of weak Pt−Pt and multicenter bonding. Lone pairs are visible as deep-red sickles on the atoms. The remaining colors (lighter blue, blue, and deep blue) corresponding to 0.0 < LOL < 0.5 represent regions in space that are increasingly avoided by electrons, such as the space far away from nuclei and the space between the shells of the atoms.

Natural Bond Orbital (NBO) Analysis and Oxidation States of the Pt Metal Centers. ^{195}Pt NMR Chemical Shifts. To shed more light on the Pt−Pt bonding situation in compounds **M1**−**M3**, a bonding analysis was carried out within the framework of the NBO analysis method.[49] The estimated natural atomic charges, natural electron configurations (Nec) of the Pt metal centers, Wiberg bond orders (WBOs) for the Pt−Pt bonds, along with the ^{195}Pt chemical shifts calculated at the GIAO/PBE0/SARCZORA(Pt)∪6-31G**(E) level, are collected in Figure 7.

The WBO values for the Pt^1−Pt^2 bonds in compounds **M1** and **M2** and for the Pt^2−Pt^3 bond in compound **M3** found in the range of 0.164−0.307 confirm the existence of strong Pt−Pt interactions. It should be noted that a WBO(Pt−Pt) value of around 1 corresponds to a single bond. On the other hand, the Nec of the Pt metal centers indicated participation of the 6s, 5d, and 6p AOs of the Pt centers in the bonding in all complexes **M1**−**M5**. The participation of 6s orbitals accounts for the direct $^1J_{Pt,Pt}$ observed for such complexes. The calculated ^{195}Pt chemical shifts were found in the range of −6560 to −6701 ppm for the Pt^2(I) metal centers in complexes **M1** and **M2** and the Pt^3(I) metal center in complex **M3**, −5893 to −6243 ppm for the Pt^1(III) centers in complexes **M1** and **M2** and the Pt^2(III) center in complex **M3**, and −4385 to −5047 ppm for the Pt^1(II) centers in **M3** and in all Pt^{II} centers in complexes **M4** and **M5**.

To estimate the oxidation states of the Pt centers in complexes **M1**−**M5**, we calculated the natural charge transferred from the ligands to the metal centers, and the results are compiled in Figure 8.

The charge transferred from the ligands toward the metal centers was estimated as the difference between the total natural charges on the "free-standing" and coordinated ligands. The natural charge transferred combined with the natural atomic charges on the Pt centers allowed us to assign the oxidation states of the Pt centers in complexes **M1**−**M5**. For complexes **M1**−**M3**, according to the LOL profiles, the bonding electron pairs of the dative coordination bonds are closer to the more electrophilic Pt^{III} centers than the less electrophilic Pt^{I} centers. Therefore, the charge transferred from the bridging PMe_2 moieties toward the more electrophilic Pt^1(III) centers in **M1** and **M2** and Pt^2(III) in **M3** should be higher than that toward the less electrophilic Pt^2(I) centers in

dx.doi.org/10.1021/ic3021639 | Inorg. Chem. 2013, 52, 1942−1953

M1 and **M2** and the Pt^3(I) center in **M3**. Moreover, according to the electroneutrality principle, the dative coordination P−Pt^{III} bonds exhibit higher ionic character than the P−Pt^I ones, thus rendering the Pt^{III} centers better acceptors of electron density from the bridging electron-donor phosphanido ligands than the Pt^I centers. Accordingly, the charges transferred from the ligands toward the Pt metal centers mapped in Figure 8 allowed the assignment of the respective oxidation states on the Pt metal centers.

CONCLUDING REMARKS

The trinuclear 48 VEC **A**, having a linear skeleton, phosphanido groups as bridging ligands, and four-coordinated metal centers (without any Pt−Pt bond), is transformed into the unsaturated **1** (46 VEC) by substitution of the acac ligand by PPh_3. In complex **1**, two Pt centers are four-coordinated and one is three-coordinated. Such unsaturation of the skeleton entails the formation of a Pt−Pt bond.[11,15,50] The process is reversible because the addition of a ligand (PPh_3 or pyridine) to the red and unsaturated **1** forms the yellow and saturated complexes **2** and **3**, respectively. The trinuclear **1** reacts also with electrophiles. Although **1** reacts with $[AgPPh_3]^+$, in a 1:1 molar ratio, we were not able to isolate the adduct $[\mathbf{1}\cdot AgPPh_3]^+$, which should be expected to be formed through a 3c-2e P^4−Pt^3−Ag bond. On the contrary, we have obtained a mixture of complexes $[(C_6F_5)_2Pt^{III}(\mu\text{-}PPh_2)_2Pt^{III}(\mu\text{-}PPh_2)_2Pt^{II}(PPh_3)_2]^{2+}$ and $[(C_6F_5)_2Pt^{II}(\mu\text{-}PPh_2)_2Pt^{II}(\mu\text{-}PPh_2)_2Pt^{II}(PPh_3)_2]$, which are the final result of the coordination of PPh_3 and the oxidation by Ag^+. The electron-rich character of the Pt^3−μ-P^4 bond, i.e., the nucleophilic character of **1**, is demonstrated by its reaction with $[Pt(C_6F_5)_2(THF)_2]$, which yields the tetranuclear **4**. Formation of the adduct $[\mathbf{1}\cdot Pt(C_6F_5)_2]$, followed by some ligand rearrangement,[42−44,51] can safely explain the isolation of **4**.

The strong intermetallic interactions resulting in a Pt^2−Pt^3 metal−metal bond along with the respective bonding mechanism were verified by employing a multitude of computational techniques (NBO analysis, Laplacian of the electron density, and LOL profiles). The oxidation states of the Pt centers in the complexes under investigation were estimated by calculation of the natural charges transferred from the ligands toward the Pt metal centers combined with the natural atomic charges acquired by the Pt centers.

From ^{195}Pt NMR spectra and theoretical calculations, it can be inferred that the oxidation states of the Pt atoms in the trinuclear metal core are [Pt^{II}, Pt^{II}, Pt^{II}] in $[(C_6F_5)_2Pt(\mu\text{-}PPh_2)_2Pt(\mu\text{-}PPh_2)_2Pt(O,O\text{-acac})]^-$ but should be considered [Pt^{II}, Pt^{III}, Pt^I] in **1**.

EXPERIMENTAL SECTION

General Comments. C, H, and N analyses were performed with a Perkin-Elmer 240B microanalyzer. IR spectra were recorded on a Perkin-Elmer Spectrum One spectrophotometer (Nujol mulls between polyethylene plates in the range 4000−350 cm^{-1}). NMR spectra were recorded on a Bruker Avance 400 spectrometer with $CFCl_3$, 85% H_3PO_4, and H_2PtCl_6 as external references for ^{19}F, ^{31}P, and ^{195}Pt, respectively. Literature methods were used to prepare the starting materials $[NBu_4][(C_6F_5)_2Pt(\mu\text{-}PPh_2)_2Pt(\mu\text{-}PPh_2)_2Pt(acac)]$[31] and *cis*-$[Pt(C_6F_5)_2(THF)_2]$.[40]

Safety Note. ***Caution!*** *Perchlorate salts of metal complexes with organic ligands are potentially explosive. Only small amounts of materials should be prepared, and these should be handled with great caution.*

*Synthesis of [$(C_6F_5)_2Pt(\mu\text{-}PPh_2)_2Pt(\mu\text{-}PPh_2)_2Pt(PPh_3)$] (**1**).* Solid $[PPh_3H][ClO_4]$[52] (0.090 g, 0.250 mmol) was added to a yellow solution of $[NBu_4][(C_6F_5)_2Pt(\mu\text{-}PPh_2)_2Pt(\mu\text{-}PPh_2)_2Pt(O,O\text{-acac})]$ (**A**; 0.500 g, 0.250 mmol) in CH_2Cl_2 (30 mL). The solution, which instantaneously turned red, was stirred for 30 min at room temperature. The red solution was passed through silica (ca. 15 cm × 2 cm^2) and evaporated to ca. 2 mL. The addition of *n*-hexane (ca. 2 mL) caused the precipitation of **1** as red crystals, which were filtered and washed with *n*-hexane (3 × 0.5 mL). Yield: 0.317 g, 66%. Anal. Found (calcd for $C_{78}F_{10}H_{55}P_5Pt_3$): C, 48.71 (48.73); H, 2.86 (2.88). IR (cm^{-1}): 785 and 778 (X-sensitive C_6F_5).[53,54] ^{19}F NMR ($CDCl_3$, 298 K, 282.4 MHz): −119.0 (*o*-F, $^3J_{^{195}Pt,F}$ = 312 Hz), −168.1 (*m*-F + *p*-F). $^{31}P\{^1H\}$ NMR ($CDCl_3$, 298 K, 161.9 MHz): δ 236.7 ($P^{3,4}$, $^1J_{Pt^3,P}$ = 2789, $^1J_{Pt^2,P}$ = 1111 Hz), 42.5 (P^5, $^1J_{Pt^3,P}$ = 5440 Hz), −158.9 ($P^{1,2}$, $^1J_{Pt^1,P}$ = 1860, $^1J_{Pt^2,P}$ = 1738 Hz). ^{195}Pt NMR ($CDCl_3$, 298 K, 85.6 MHz): δ −3712 (Pt^1, m), −4720 (Pt^2, tt), −5228 (Pt^3, dt, $^1J_{Pt^2,Pt^3}$ = 515 Hz).

*Synthesis of [$(C_6F_5)_2Pt(\mu\text{-}PPh_2)_2Pt(\mu\text{-}PPh_2)_2Pt(PPh_3)(L)$] [L = PPh_3 (**2**), py (**3**)].* PPh_3 (0.050 g, 0.190 mmol) or py (0.1 mL, 1.2 mmol) was added to a red solution of **1** (0.200 g, 0.104 mmol) in CH_2Cl_2 (10 mL). The color of the solution instantaneously turned yellow, and a yellow solid precipitated, **2** or **3**. The solid was filtered and washed with cold CH_2Cl_2 (3 × 0.5 mL). Yield of **2**:[28] 0.197 g, 87%. Yield of **3**: 0.175 g, 84%. Anal. Found (calcd for $C_{83}F_{10}H_{60}NP_5Pt_3$): C, 49.60 (49.81); H, 2.81 (3.02); N, 0.63 (0.70). IR (cm^{-1}): 1603 (pyridine); 780 and 771 (X-sensitive C_6F_5).

Reaction of 1 with *cis*-[$Pt(C_6F_5)_2(THF)_2$]. *cis*-$[Pt(C_6F_5)_2(THF)_2]$ (0.035 g, 0.052 mmol) was added to a red solution of **1** (0.100 g, 0.052 mmol) in CH_2Cl_2 (15 mL). The solution was stirred for 24 h and evaporated to ca. 0.5 mL. $CHCl_3$ (2 mL) and *n*-hexane (10 mL) were added with stirring. An orange solid precipitated and was filtered and washed with *n*-hexane (3 × 1 mL, 0.085 g). The $^{31}P\{^1H\}$ NMR ($CDCl_3$, 298 K) spectrum of the solid is mainly **4**,[42] together with **1** (ca. 20%).

X-ray Structure Determination of $\mathbf{1}\cdot 0.25CHCl_3\cdot 0.25C_6H_{14}$. Crystal data and other details of structure analysis are presented in Table 3. Suitable crystals for X-ray diffraction studies were obtained by slow diffusion of *n*-hexane into a concentrated solution of complex **1** in 3 mL of $CHCl_3$. The crystal was mounted at the end of a quartz fiber. The radiation used in all cases was graphite-monochromated Mo Kα (α = 0.71073 Å). X-ray intensity data were collected on a Bruker Smart

Table 3. Crystal Data and Structure Refinement for Complex $\mathbf{1}\cdot 0.25CHCl_3\cdot 0.25C_6H_{14}$

formula	$C_{78}H_{55}F_{10}P_5Pt_3\cdot 0.25CHCl_3\cdot 0.25C_6H_{14}$
M_t [g mol^{-1}]	1973.73
T [K]	100(1)
λ [Å]	0.71073
cryst syst	monoclinic
space group	$P2_1/n$
a [Å]	16.0336(11)
b [Å]	19.2639(13)
c [Å]	19.2639(13)
β [deg]	101.592(1)
V [$Å^3$]	7035.1(8)
Z	4
ρ [g cm^{-3}]	1.863
μ [mm^{-1}]	6.165
F(000)	3796
2θ range [deg]	2.8−50.1
no. of reflns collected	37505
no. of unique reflns	12373
R(int)	0.0593
final R indices [$I > 2\sigma(I)$][a]	R1 = 0.0360, wR2 = 0.0568
R indices (all data)	R1 = 0.0529, wR2 = 0.0588
GOF on F^2[b]	0.991

[a] $R1 = \sum(|F_o| - |F_c|)/\sum|F_o|$. $wR2 = [\sum w(F_o^2 - F_c^2)^2/\sum w(F_o^2)^2]^{1/2}$. [b] $GOF = [\sum w(F_o^2 - F_c^2)^2/(n_{obs} - n_{param})]^{1/2}$.

dx.doi.org/10.1021/ic3021639 | *Inorg. Chem.* 2013, 52, 1942−1953

Apex diffractometer. The diffraction frames were integrated using the *SAINT* program[55] and the reflections corrected from absorption with *SADABS*.[56]

The structures were solved by Patterson and Fourier methods and refined by full-matrix least squares on F^2 with *SHELXL-97*.[57] All non-H atoms were assigned anisotropic displacement parameters and refined without positional constraints, except as noted below. All H atoms were constrained to idealized geometries and assigned isotropic displacement parameters equal to 1.2 times the U_{iso} values of their attached parent atoms (1.5 times for the methyl H atoms). Molecules of chloroform and *n*-hexane solvents were found, located in the same area of the cell, near an inversion center and modeled with a partial occupancy of 0.25. For these solvent molecules, the interatomic distances were restrained to sensible values and a common thermal anisotropic set of parameters was used for the C atoms of *n*-hexane. Full-matrix least-squares refinement of these models against F^2 converged to the final residual indices given in Table 3.

COMPUTATIONAL DETAILS

The geometries of all stationary points were fully optimized, without symmetry constraints, employing the 1997 hybrid functional of Perdew, Burke, and Ernzerhof,[58] as implemented in the *Gaussian03* program suite.[59] This functional uses 25% exchange and 75% correlation weighting and is denoted as PBE0. The selection of the PBE0 functional was based on the fact that PBE0 generally gives the best results for various properties of transition-metal, lanthanide, actinide, and main-group-element compounds.[60−63] For the geometry optimizations, we used the Def2-TZVP basis set for Pt and 6-31G**(E) for all other nonmetal atoms E. Hereafter the method used in DFT calculations is abbreviated as PBE0/Def2-TZVP(Pt)U6-31**G(E) (E = nonmetal element). All stationary points have been identified as minima (number of imaginary frequencies NImag = 0).

NBO population analysis was performed using Weinhold's methodology.[49,64] Magnetic shielding tensors have been computed with the gauge-including atomic orbitals (GIAO) DFT method,[65,66] as implemented in the *Gaussian03* series of programs[59] employing the PBE0 level of theory combined with the SARCZORA basis set[67,68] for Pt and 6-31**(E) for all other nonmetal elements E. The Laplacian of electron density and the LOL plots were obtained by employing the *Multiwfn* software version 2.2.1.[69]

ASSOCIATED CONTENT

Supporting Information

Crystallographic data of **1**·0.25$CHCl_3$·0.25C_6H_{14}) in CIF format, some NMR spectra, and Cartessian coordinates and energies of **M1**−**M5**. This material is available free of charge via the Internet at http://pubs.acs.org.

AUTHOR INFORMATION

Corresponding Author

*E-mail: cfortuno@unizar.es (C.F.), p.mastrorilli@poliba.it (P.M.), attsipis@uoi.gr (A.T.).

Notes

The authors declare no competing financial interest.

Polynuclear Homo- or Heterometallic Palladium(II)−Platinum(II) Pentafluorophenyl Complexes Containing Bridging Diphenylphosphido Ligands. 30. For part 29, see ref 1.

ACKNOWLEDGMENTS

This work was supported by the Spanish MICINN (DGI)/FEDER (Project CTQ2008-06669-C02-01/BQU) and the Gobierno de Aragón (Grupo de Excelencia: Química Inorgánica y de los Compuestos Organometálicos). S.I. gratefully acknowledges a grant provided by the Ministerio de Educación y Ciencia. A.T. thanks the University of Ioannina for a sabbatical leave and all colleagues at the Departamento de Química Inorgánica, Instituto de Síntesis Química y Catálisis Homogénea, Facultad de Ciencias, Universidad de Zaragoza, CSIC, Zaragoza (Spain), for their generous hospitality. Italian MIUR (PRIN Project 2009LR88XR) and COST Phosphorus Science Network (PhoSciNet, Project CM0802) are also gratefully acknowledged.

REFERENCES

(1) Arias, A.; Forniés, F.; Fortuño, C.; Martín, A.; Latronico, M.; Mastrorilli, P.; Todisco, S.; Gallo, V. *Inorg. Chem.* **2012**, *51*, 12628−12696.
(2) Mastrorilli, P. *Eur. J. Inorg. Chem.* **2008**, 4835−4850.
(3) Bender, R.; Okio, C.; Welter, R.; Braunstein, P. *Dalton Trans.* **2009**, 4901−4907.
(4) Cavazza, C.; Fabrizi de Biani, F.; Funaioli, T.; Leoni, P.; Marchetti, F.; Marchetti, L.; Zanello, P. *Inorg. Chem.* **2009**, *48*, 1385−1397.
(5) Gallo, V.; Latronico, M.; Mastrorilli, P.; Nobile, C. F.; Suranna, G. P.; Ciccarella, G.; Englert, U. *Eur. J. Inorg. Chem.* **2005**, 4607−4616.
(6) Latronico, M.; Polini, F.; Gallo, V.; Mastrorilli, P.; Calmuschi-Cula, B.; Englert, U.; Re, N.; Repo, T.; Räisänen, M. *Inorg. Chem.* **2008**, *47*, 9779−9796.
(7) Archambault, C.; Bender, R.; Braunstein, P.; Dusausoy, Y. *J. Chem. Soc., Dalton Trans.* **2002**, 4084−4090.
(8) Albinati, A.; Balzanot, F.; Fabrizi de Biani, F.; Leoni, P.; Manca, G.; Marchetti, L.; Rizzato, S.; Barretta, U. G. *Inorg. Chem.* **2010**, *49*, 3714−3720.
(9) Gallo, V.; Latronico, M.; Mastrorilli, P.; Nobile, C. F.; Polini, F.; Re, N.; Englert, U. *Inorg. Chem.* **2008**, *47*, 4785−4795.
(10) Alonso, E.; Casas, J. M.; Cotton, F. A.; Feng, X. J.; Forniés, J.; Fortuño, C.; Tomás, M. *Inorg. Chem.* **1999**, *38*, 5034−5040.
(11) Falvello, L. R.; Forniés, J.; Fortuño, C.; Durán, F.; Martín, A. *Organometallics* **2002**, *21*, 2226−2234.
(12) Alonso, E.; Forniés, J.; Fortuño, C.; Martín, A.; Orpen, A. G. *Organometallics* **2003**, *22*, 5011−5019.
(13) Ara, I.; Chaouche, N.; Forniés, J.; Fortuño, C.; Kribii, A.; Tsipis, A. C. *Organometallics* **2006**, *25*, 1084−1091.
(14) Berenguer, J. R.; Chaouche, N.; Forniés, J.; Fortuño, C.; Martín, A. *New J. Chem.* **2006**, *30*, 473−478.
(15) Forniés, J.; Fortuño, C.; Gil, R.; Martín, A. *Inorg. Chem.* **2005**, *44*, 9534−9541.
(16) Forniés, J.; Fortuño, C.; Ibáñez, S.; Martín, A. *Inorg. Chem.* **2006**, *45*, 4850−4858.
(17) Forniés, J.; Fortuño, C.; Ibáñez, S.; Martín, A.; Tsipis, A. C.; Tsipis, C. A. *Angew. Chem., Int. Ed.* **2005**, *44*, 2407−2410.
(18) Forniés, J.; Fortuño, C.; Ibáñez, S.; Martín, A.; Romero, P.; Mastrorilli, P.; Gallo, V. *Inorg. Chem.* **2011**, *50*, 285−298.
(19) Latronico, M.; Mastrorilli, P.; Gallo, V.; Dell'Anna, M. M.; Creati, F.; Re, N.; Englert, U. *Inorg. Chem.* **2011**, *50*, 3539−3558.
(20) Mastrorilli, P.; Latronico, M.; Gallo, V.; Polini, F.; Re, N.; Marrone, A.; Gobetto, R.; Ellena, S. *J. Am. Chem. Soc.* **2010**, *132*, 4752−4765.
(21) Dell'Anna, M. M.; Giardina-Papa, D.; Ibáñez, S.; Martín, A.; Mastrorilli, P.; Nobile, C. F.; Peruzzini, M. *Eur. J. Inorg. Chem.* **2009**, 4454−4463.
(22) Mastrorilli, P. *Dalton Trans.* **2008**, 4555−4557.
(23) Dell'Anna, M. M.; Mastrorilli, P.; Nobile, C. F.; Calmuschi-Cula, B.; Englert, U.; Peruzzini, M. *Dalton Trans.* **2008**, 6005−6013.
(24) Dell'Anna, M. M.; Englert, U.; Latronico, M.; Luis, P. L.; Mastrorilli, P.; Giardina-Papa, D.; Nobile, C. F.; Peruzzini, M. *Inorg. Chem.* **2006**, *45*, 6892−6900.
(25) Mastrorilli, P.; Nobile, C. F.; Fanizzi, F. P.; Latronico, M.; Hu, C.; Englert, U. *Eur. J. Inorg. Chem.* **2002**, 1210−1218.
(26) Mastrorilli, P.; Palma, M.; Nobile, C. F.; Fanizzi, F. P. *J. Chem. Soc., Dalton Trans.* **2000**, 4272−4276.
(27) Giannandrea, R.; Mastrorilli, P.; Nobile, C. F.; Englert, U. *J. Chem. Soc., Dalton Trans.* **1997**, 1355−1358.

(28) Forniés, F.; Fortuño, C.; Ibáñez, S.; Martín, A.; Mastrorilli, P.; Gallo, V. *Inorg. Chem.* **2011**, *50*, 10798−10809.
(29) Aullón, G.; Alemany, P.; Álvarez, S. *J. Organomet. Chem.* **1994**, *478*, 75−82.
(30) Falvello, L. R.; Forniés, J.; Fortuño, C.; Martínez, F. *Inorg. Chem.* **1994**, *33*, 6242−6246.
(31) Ara, I.; Forniés, J.; Fortuño, C.; Ibáñez, S.; Martín, A.; Mastrorilli, P.; Gallo, V. *Inorg. Chem.* **2008**, *47*, 9069−9080.
(32) Palacios, A. A.; Alemany, P.; Alvarez, S. *J. Chem. Soc., Dalton Trans.* **2002**, 2235−2243.
(33) Mealli, C.; Ienco, A.; Galindo, A.; Pérez-Carreño, E. *Inorg. Chem.* **1999**, *38*, 4620−4625.
(34) Albinati, A.; Leoni, P.; Marchetti, F.; Marchetti, L.; Pasquali, M.; Rizzato, S. *Eur. J. Inorg. Chem.* **2008**, 4092−4100.
(35) Taylor, N. J.; Chieh, P. C.; Carty, A. J. *J. Chem. Soc., Chem. Commun.* **1975**, 448−449.
(36) Alonso, E.; Casas, J. M.; Forniés, J.; Fortuño, C.; Martín, A.; Orpen, A. G.; Tsipis, C. A.; Tsipis, A. C. *Organometallics* **2001**, *20*, 5571−5582.
(37) Still, B. M.; Kumar, P. G. A.; Aldrich-Wright, J. R.; Price, W. S. *Chem. Soc. Rev.* **2007**, *36*, 665−686 and references cited therein.
(38) Pregosin, P.; Kunz, R. W. *^{31}P and ^{13}C NMR of Transition Metal Phosphine Complexes*; Springer-Verlag: Berlin, 1979.
(39) Alonso, E.; Forniés, F.; Fortuño, C.; Lledós, A.; Martín, A.; Nova, A. *Inorg. Chem.* **2009**, *48*, 7679−7690.
(40) Usón, R.; Forniés, F.; Tomás, M.; Menjón, B. *Organometallics* **1985**, *4*, 1912−1914.
(41) Ara, I.; Chaouche, N.; Forniés, J.; Fortuño, C.; Kribii, A.; Martín, A. *Eur. J. Inorg. Chem.* **2005**, 3894−3901.
(42) Alonso, E.; Forniés, J.; Fortuño, C.; Martín, A.; Orpen, A. G. *Organometallics* **2003**, *22*, 2723−2728.
(43) Alonso, E.; Forniés, J.; Fortuño, C.; Martín, A.; Orpen, A. G. *Chem. Commun.* **1996**, 231−232.
(44) Alonso, E.; Forniés, J.; Fortuño, C.; Martín, A.; Orpen, A. G. *Organometallics* **2000**, *19*, 2690−2697.
(45) Bader, R. F. W. *Chem. Rev.* **1991**, *91*, 893−928.
(46) Popov, A. A.; Dunsch, L. *Chem.—Eur. J.* **2009**, *15*, 9707−9729.
(47) Schmider, H. L.; Becke, A. D. *J. Mol. Struct. (THEOCHEM)* **2000**, *527*, 51−61.
(48) Schmider, H. L.; Becke, A. D. *J. Chem. Phys.* **2002**, *116*, 3184−3193.
(49) Reed, A. E.; Curtiss, L. A.; Weinhold, F. *Chem. Rev.* **1988**, *88*, 899−926.
(50) Forniés, J.; Fortuño, C.; Ibáñez, S.; Martín, A. *Inorg. Chem.* **2008**, *47*, 5978−5987.
(51) Chaouche, N.; Forniés, J.; Fortuño, C.; Kribii, A.; Martín, A. *J. Organomet. Chem.* **2007**, *692*, 1168−1172.
(52) Zhu, J.; Dai, J.-X.; Zhang, Q.-F. *Acta Crystallogr.* **2007**, *E63*, o363−o364.
(53) Usón, R.; Forniés, J. *Adv. Organomet. Chem.* **1988**, *28*, 219−297.
(54) Maslowsky, E. J. *Vibrational Spectra of Organometallic Compounds*; Wiley: New York, 1997.
(55) *SAINT*, version 5.0; Bruker Analytical X-ray Systems: Madison, WI, 1997.
(56) Sheldrick, G. M. *SADABS: empirical absorption program*; University of Göttingen: Göttingen, Germany, 1996.
(57) Sheldrick, G. M. *SHELXL-97: a program for crystal structure determination*; University of Göttingen: Göttingen, Germany, 1997.
(58) Perdew, J. P.; Burke, K.; Ernzerhof, M. *Phys. Rev. Lett.* **1996**, *77*, 3865−3868.
(59) Frisch, M. J.et al. *Gaussian03*, revision B.03; Gaussian, Inc.: Pittsburgh, PA, 2003. See the Supporting Information for the full reference.
(60) Vetere, V.; Adamo, C.; Maldivi, P. *Chem. Phys. Lett.* **2000**, *325*, 99−105.
(61) Graciani, J.; Marquez, A. M.; Plata, J. J.; Ortega, Y.; Hernández, N. C.; Meyer, A.; Zicovich-Wilson, C. M.; Sanz, J. F. *J. Chem. Theory Comput.* **2011**, *7*, 56−65.
(62) Zahn, S.; Kirchner, B. *J. Phys. Chem. A* **2008**, *112*, 8430−8435.
(63) Vlaisavljevich, B.; Mir, P.; Cramer, C. J.; Gagliardi, L.; Infante, I.; Liddle, S. T. *Chem.—Eur. J.* **2011**, *17*, 8424−8433.
(64) Weinhold, F. In *The Encyclopedia of Computational Chemistry*; Schleyer, P. v. R., Ed.; John Wiley & Sons: Chichester, U.K., 1998.
(65) Ditchfield, R. *Mol. Phys.* **1974**, *27*, 789−809.
(66) Gauss, J. *Chem. Phys.* **1993**, *99*, 3629−3643.
(67) Pantazis, D. A.; Chen, X.-Y.; Landis, C. R.; Neese, F. *J. Chem. Theory Comput.* **2008**, *4*, 908−919.
(68) EMSL basis set exchange, https://bse.pnl.gov/bse/portal, accessed April 28, 2011.
(69) Lu, T.; Chen, F. *J. Comput. Chem.* **2012**, *33*, 580−592.